Editors' Suggestion

Wavelength-Tunable Quantum Absorption Spectroscopy in the Broadband Midinfrared Region

Masaya Arahata,[1] Yu Mukai,[1] Toshiyuki Tashima,[1] Ryo Okamoto,[1,2] and Shigeki Takeuchi[1,*]

[1] *Department of Electronic Science and Engineering, Kyoto University, Kyotodaigakukatsura, Nishikyo-ku, Kyoto 615-8510, Japan*

[2] *Japan Science and Technology Agency, PRESTO, Gobancho, Chiyoda-ku, Tokyo 102-0076, Japan*

(Received 22 March 2022; accepted 1 August 2022; published 7 September 2022)

Harnessing the quantum interference between generation processes of visible-infrared photon pairs, infrared quantum absorption spectroscopy (IRQAS) enables the estimation of the optical properties of a medium in the infrared region from interferograms obtained by detecting visible photons. Since IRQAS enables infrared spectroscopy without using a light source or detector in the infrared region, infrared spectrometers can be made more compact and less invasive, which will find many alternative applications. A broader spectroscopy bandwidth is key, however, the spectral bandwidths of the reported IRQAS system have been limited to less than 1 μm so far. Here, we report a wavelength-tunable IRQAS system covering the spectral range of 1.9–5.2 μm with a bandwidth of 3.3 μm. In this system, the wavelengths of spontaneous parametric down-conversion photon pairs are tuned by rotating a nonlinear crystal with respect to the pump beam. Rapid spectral measurements (coarse scan) over a broad bandwidth (1.9–5.2 μm) is successfully demonstrated using silica glass as a sample, and the obtained spectrum clearly shows OH-stretching absorption bands, which agreed well with the result measured by a conventional infrared spectrometer. Furthermore, quantum Fourier-transform infrared spectroscopy measurements are demonstrated for these absorption bands with a high resolution (fine scan). The reported concept of the ultrabroadband IRQAS system paves the way for the use of IRQAS in real-world applications.

DOI: 10.1103/PhysRevApplied.18.034015

I. INTRODUCTION

Infrared spectroscopy is a powerful technique that can be used to analyze the composition and structure of samples by obtaining information on the vibrational and rotational modes of molecules [1]. Fourier-transform infrared (FTIR) spectroscopy can collect high-resolution spectral data over a wide wavelength range [2]. There are many potential or apparent needs for compact, portable, highly sensitive infrared spectrometers, for example, the examination of chemicals in various outdoor environments or security checks, and as built-in monitoring equipment in chemical plants or semiconductor manufacturing equipment. However, traditional infrared spectroscopy has some technical problems for further miniaturization. One problem exists in a current infrared light source. Traditional infrared spectroscopy uses a heater (ceramic of SiC) as a broadband infrared light source, however, the heat from the source is a serious problem for the miniaturization. In addition, such light sources are not very stable and not efficient. Another problem exists in the infrared detector. The sensitivity of the infrared detector is limited due to the room-temperature thermal radiation and their SNR is poorer when compared to visible-light detectors such as silicon photodetectors.

Infrared quantum absorption spectroscopy (IRQAS) [3] is one of the quantum sensing technologies [4–6] utilizing the quantum interference between the generation processes of visible-infrared entangled photon pairs [7–9]. The absorbance of samples in the infrared region is obtained from an interferogram of visible photon-detection signals. Since IRQAS enables infrared spectroscopy without using a light source or detector in the infrared region, infrared spectrometers can be made more compact and much less invasive. Note that the IRQAS is based on SU(1, 1) interferometers [8,10,11] operated in the low-gain regime, where the average photon flux is below one per correlation time of biphotons, this interference effect cannot be interpreted by a classical theory.

Although a broader bandwidth of the spectroscopy is essential for various applications, the spectral bandwidths of the reported IRQAS systems have been limited to less than 1 μm so far. The first IRQAS was experimentally demonstrated by Kalashnikov *et al.* [3]. They measured the absorption coefficient and refractive index for CO_2 gas in the wavelength region 4.0–4.5 μm from the interference

*takeuchi@kuee.kyoto-u.ac.jp

fringes of visible photons with a visible laser and CCD camera. Recently, IRQAS systems have been developed for imaging [12–14] and gas sensing [15,16] in the mid-infrared (MIR) region; however, the bandwidths of the spectrometers have been limited to less than 1 μm due to the small spectral bandwidth associated with photon-pair generation. Recently, interesting attempts to widen the spectral bandwidth using broadband group-velocity phase matching was reported [16–18] and a spectral bandwidth of 0.9 μm has been reported.

Here, we report a wavelength-tunable IRQAS system covering the spectral range of 1.9–5.2 μm with a bandwidth of 3.3 μm. In this system, the wavelengths of spontaneous parametric down-conversion (SPDC) photon pairs are tuned in the wavelength region of 1.9–5.2 μm by rotating a nonlinear crystal with respect to the pump beam [19]. Quantum interference is well maintained for the whole region without additional fine realignment. To evaluate the performance of the IRQAS system, we experimentally demonstrate transmission spectrum measurements of a silica glass sample. For rapid spectral measurements with a broad bandwidth (coarse scan), we evaluate the transmittance of a sample from the change in the visibility of the quantum interferogram by scanning the wavelength of the signal and the idler photons. The obtained result over the spectral range of 1.9–5.2 μm clearly shows absorption bands due to OH stretching, and agreed well with the spectrum measured by conventional FTIR spectroscopy. Furthermore, quantum Fourier-transform infrared spectroscopy (QFTIR) [9] measurements, where the transmission spectra are obtained from Fourier analysis of quantum interferograms, are demonstrated for the absorption bands with a higher resolution of 8.33 cm^{-1} (fine scan). The reported concept of the ultrabroadband IRQAS system paves the way for the use of IRQAS in real-world applications.

The rest of the paper is constructed as follows. In Sec. II, we propose two analytical methods realized in a wavelength-tunable IRQAS system: the coarse scan and fine scan methods. In Sec. III, we present the experimental setup for a wavelength-tunable IRQAS system with continuous crystal rotation. In Sec. IV, we evaluate the performance of the IRQAS system from the measurement results for quantum interferograms over the MIR region 2–5 μm. We also experimentally demonstrate a rapid transmission spectrum measurement method using a coarse scan, and a high-resolution measurement method using a fine scan (QFTIR). Section V summarizes the points of this work and presents the conclusions.

II. ANALYTICAL METHODS

In this section, we describe two methods for transmission spectrum measurement, the coarse-scan and fine-scan methods. In the coarse-scan method, the infrared transmittance is evaluated from the ratio of the visibilities of quantum interferograms taken with and without a sample. In this method, the probe wavelength can be scanned continuously by angle tuning of the SPDC photon-pair generation. This measurement scheme allows transmittance measurements over a wide MIR region of 2–5 μm within a short acquisition time. However, the wavelength resolution is limited by the spectral bandwidth of photon pairs. In the fine-scan method, based on QFTIR measurements, the transmission spectrum is obtained via a Fourier analysis of an interferogram with a higher resolution. The wavelength resolution can be improved by expanding the range of the optical path length difference of the interferometer arms.

First, following the discussion in Refs. [16,20], we provide an analytical expression for the quantum interferogram, i.e., the modulation of the signal photon count rate due to quantum interference between visible-infrared photon pairs. For simplicity, we assume that pump photons have a monochromatic frequency ω_p and signal and idler photons are generated into frequency modes ω_s and ω_i only in the collinear condition. In a Michelson-type quantum interferometer, as shown in Fig. 1 (details in Sec. III), the signal count rate at the detector is expressed as

$$P_s \propto 2 + \int_0^\infty d\omega_i |F(\omega_i)|^2 \{[\tau^*(\omega_i)]^2 e^{-i\omega_i \Delta t} e^{i\Theta} + \text{c.c.}\}, \tag{1}$$

where $\Delta t = t_s - t_i$ is the time delay between the propagation time of the signal t_s and idler t_i photons in the interferometer, $\tau(\omega_i) = |\tau(\omega_i)| e^{i\phi_i(\omega_i)}$ is the complex amplitude transmittance coefficient for the sample including the phase shift $\phi_i(\omega_i) \propto \omega_i[n(\omega_i) - 1]l/c$, where l is the

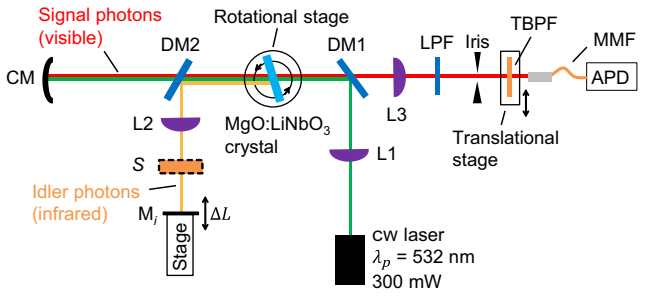

FIG. 1. Experimental setup for wavelength-tunable IRQAS system with continuous crystal rotation. L1, focusing lens for pump (f = 200 mm); DM1, dichroic mirror with 567-nm cut-on wavelength (DMLP567, Thorlabs); DM2, dichroic mirror with 2000-nm cut-off wavelength; CM, concave mirror (f = 100 mm); L2, collimation lens for idler (f = 100 mm); S, sample; M_i, mirror for idler; L3, collimation lens for signal (f = 250 mm); LPF, long-pass filter with 550-nm cut-on wavelength; TBPF, tunable bandpass filter with typical bandwidths of about 20–30 nm; MMF, multimode fiber; APD, Si avalanche photodiode.

length of the sample, $n(\omega_i)$ is the real part of the refractive index, c is the speed of light, Θ is the fixed phase term independent of Δt, and $F(\omega_i)$ is a reduced expression for the two-photon amplitude obtained from the energy conservation and the monochromatic pump condition [9]. We use the normalization condition for the two-photon amplitude, $\int d\omega_i |F(\omega_i)|^2 = 1$. Equation (1) shows that the quantum interference of generated signal photons depends on the optical loss and phase retardation of the idler photons in the sample.

A. Coarse scan

For a rapid spectral measurement with a broad bandwidth (coarse scan), we evaluate the transmittance of a sample from the change in the visibility of the quantum interferograms, scanning the wavelength of the signal and the idler photons. Expressing the idler frequency as $\omega_i = \omega_{i0} - \Omega$, where ω_{i0} is the idler central wavelength and Ω is the detuning frequency, and rewriting Eq. (1) with the optical path length difference $\Delta L = c\Delta t$, we obtain

$$P_s(\Delta L) \propto 2 + 2T|\mu(\Delta L)| \cos\left[\frac{\omega_{i0}}{c}\Delta L - \Theta\right], \quad (2)$$

$$\mu(\Delta L) = \int d\Omega |F'(\Omega)|^2 e^{i2\phi_i'(\Omega)} e^{-i(\Omega/c)\Delta L}, \quad (3)$$

where $F'(\Omega)$ and $\phi_i'(\Omega)$ are the two-photon amplitude and the phase shift as a function of Ω, respectively, $\mu(\Delta L)$ is the normalized correlation function for the SPDC photon pairs [20] including the effect of the dispersion of the sample, and T is the transmittance of the sample under the assumption that it is independent from the idler wavelength. We can see that the visibility of the interference signal is not changed if the group-velocity dispersion (GVD) for the sample is small enough relative to $\mu(\Delta L)$. We assume that $\phi_i'(\Omega)$ depends only on the Taylor expansion first- and second-order terms of Ω, while the effect of the higher-order terms is small, that is, $\phi_i'(\Omega) \approx \phi_{i0} + (\beta'\Omega + \beta''\Omega^2/2)l$, where ϕ_{i0} is a constant that is independent of Ω, β' is the group delay (inverse of group velocity), and β'' is the GVD. Here, we consider the effect of dispersion due to only the GVD on the visibility of a quantum interferogram. With the spectral profile of the biphotons $F'(\Omega)$, Eq. (2) shows the envelop function for the quantum interferogram (Fig. 1). When the phases of the pump and signal photons are fixed, with an optical path length difference ΔL, the signal photon count rate P_s depends on the phase retardation of the idler photons. If the effect of dispersion in the sample on the correlation function of the SPDC photon pairs is small, then the transmittance of the sample can be extracted from the ratio of the visibilities $[= (P_{s,\max} - P_{s,\min})/(P_{s,\max} + P_{s,\min})]$ with and without the sample, given by $V/V_{\rm ref} = T$, where $V_{\rm ref}$ is the reference interference visibility including the intrinsic losses in the interferometer without a sample, and V is the interference visibility with a sample. The transmission spectrum over a wide MIR range can be obtained by iterating transmittance measurements while scanning the probe idler wavelength.

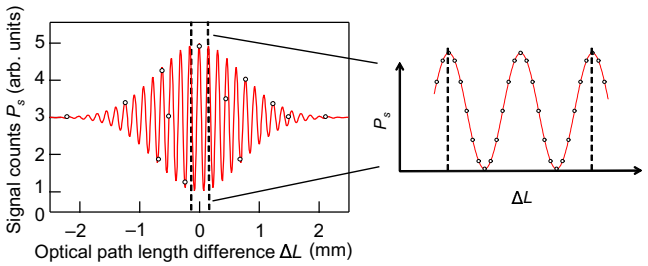

FIG. 2. Rapid spectral measurement with a broad bandwidth (coarse scan). The signal photon counts are measured for about two periods while changing the optical path length of the idler photons around the position where the amplitude of the interference fringes becomes a maximum. Then, the amplitude of the quantum interference fringes is determined. The position where the amplitude of the interference fringes is a maximum is roughly predicted based on the refractive index and thickness of the sample, and is obtained by scanning over a wide area as an initial measurement. Note that the figure does not provide experimental data.

Next, we explain the procedure for the coarse-scan method (Fig. 2). The peak of the interference signal is roughly found around zero ΔL using a large step size over a broad range of ΔL. Next, by scanning the mirror over a range of about two periods around the interference peak, we obtain the quantum interferogram amplitude. Then, inserting a sample in the idler interferometer arm, we perform the same procedure to obtain the transmittance. Note that information on the refractive index and the thickness of the sample is helpful for obtaining a rough estimate of the peak position of the interference signal. The experimental results using this method are explained in Sec. IV.

B. Fine scan using QFTIR

For the transmission spectrum measurement with higher resolution (fine scan), we use QFTIR, with reference to Ref. [9]. In the same manner as for conventional FTIR spectroscopy, the quantum interferogram is converted into a Fourier spectrum with a wave number k. Transforming the propagation time into the optical path length difference and the frequency into the wave number, in Eq. (1), we obtain

$$P_s(\Delta L) \propto 2 + \int_0^\infty dk_i |F_k(k_i)|^2 \{[\tau_k'^*(k_i)]^2 \times e^{-ik_i\Delta L} e^{i\Theta'} + \text{c.c.}\}, \quad (4)$$

where $F_k(k) = F(ck)$ and $\tau_k(k) = \tau(ck)$ are the two-photon amplitude and transmission coefficients as functions

of k, respectively, and Θ' is a fixed phase term independent of ΔL. Performing a Fourier transform of the quantum interferogram, we obtain the Fourier spectral amplitude $A_s(k)$ for the interferogram at a positive wave number $k > 0$, given by

$$A_s(k) = \frac{1}{2\pi}\int d\Delta L P_s(\Delta L)e^{ik\Delta L} \propto |F_k(k)|^2[\tau_k'^*(k)]^2 e^{i\phi}. \quad (5)$$

Here, we omit the integral of the constant value, $1/(2\pi)\int d\Delta L(2)e^{ik\Delta L}$, which is the dc component of the interference signal. The transmittance can be obtained from the ratio of the Fourier amplitudes with and without a sample, given by

$$|A_s(k)/A_s^0(k)| = |\tau_k'^*(k)|^2 = T(k), \quad (6)$$

where $T(k)$ is the transmittance of the sample at k. Equation (6) shows that it is possible to measure the transmittance of a sample at each wavelength in the SPDC spectral region. In the fine-scan method, the resolution of the measurement is determined by the maximum optical path delay due to the scanning range of the idler mirror. Therefore, the resolution of the transmission spectrum measurement with QFTIR can be increased by extending the scanning range of the idler mirror. The experimental results using this method are described in Sec. IV.

III. EXPERIMENTS

In this section, we describe the experimental setup for the wavelength-tunable IRQAS system with continuous crystal rotation as shown in Fig. 1. A 0.5-mm-thick $LiNbO_3$ crystal doped with 5-mol% MgO (LN) (CASTECH) with a cut angle of 57.9° is pumped by a cw laser beam with a wavelength of 532 nm (Cobolt Samba, power 300 mW, linewidth less than 1 MHz) at room temperature. The pump beam is focused into the crystal by a lens L1 ($f = 200$ mm). The beam diameter is 120 μm at the crystal position. Signal (visible) and idler (infrared) photons are generated via a type-I ($e \rightarrow oo$) collinear SPDC process, where the pump light with extraordinary (horizontal) polarization (e) is down-converted into signal and idler photons with ordinary (vertical) polarization (o). For a normal incidence pump beam on the crystal, signal photons with a wavelength of 692 nm and idler photons with a wavelength of 2300 nm are generated. As we reported in Ref. [19], the wavelengths of the idler photons can be tuned in the broad MIR region by rotating the crystal with respect to the pump beam. The signal and pump photons and the idler photons are separated by the dichroic mirror DM2 (Optical Coatings Japan) designed to transmit the visible photons (400–800 nm) and reflect the MIR photons (2–5 μm). Then, the signal and pump photons are together reflected back to the crystal by a silver concave mirror CM ($f = 100$ mm). The idler photons are collimated by a MIR antireflection coated (2–5 μm) lens L2 ($f = 100$ mm) and then pass through an ultraviolet fused silica glass window (UVFS) with a thickness of 1 mm as a sample and are reflected by a silver mirror M_i on a translation stage (FS-1050UPX, Sigma Koki), which is a high-accuracy feedback stage with a position repeatability of ±2 nm. The optical path length difference ΔL can be tuned by changing the position of M_i. Then, at the crystal, the second SPDC generation process occurs by the reflected pump beam. As described above, the probability amplitudes for the first and second SPDC processes interfere only when the events are indistinguishable. Note that in this experiment, the polarization of pump light and signal and idler photons are maintained in the interferometer. After being collimated by a lens L3 ($f = 250$ mm) and passing through a long-pass filter, an iris as a spatial filter, and a tunable bandpass filter (Edmund optics, linear variable bandpass filter NIR 550–1000 nm, typical bandwidth of about 20–30 nm) on a translation stage to eliminate the residual pump beam and the background light, signal photons are coupled to a multimode fiber and then guided to a Si avalanche photodiode (SPCM-AQRH-14FC, Excelitas Tech.) and a photon counter (SR400, Stanford Research Systems) to record single photon counts to observe the quantum interferogram.

IV. RESULTS

A. Evaluation of wavelength-tunable IRQAS system performance

In this section, we show the experimental results for the wavelength-tunable IRQAS system performance for transmission spectrum measurements of a sample. First, we observe the quantum interferograms in the wavelength region of 2.1–4.7 μm and evaluate the generated bandwidth of the SPDC spectra related to the resolution of the measurement. We tune the SPDC wavelength by rotating the crystal with respect to the pump beam by 1° steps from $\theta = -10°$ to 30°, where θ is the incidence angle of the pump beam, demonstrating the wavelength-tunability of this IRQAS system. Figure 3 shows the quantum interferograms P_s and the signal photon count rate recorded as a function of the optical path length difference ΔL, for signal and idler photon wavelengths of (a) 712 and 2104 nm and (b) 600 and 4694 nm, respectively. The insets in Figs. 3(a) and 3(b) show the interference fringes around $\Delta L = 0$. We translate the idler mirror M_i by step sizes of 100 nm (corresponding to a change in ΔL of 200 nm) up to a total scanning length W of 400 μm. The integration time is 300 ms for each step. It is clearly shown that the periods of the interference fringes correspond to idler wavelengths of about 2.1 and 4.7 μm. Figures 3(c) and 3(d) show the Fourier amplitude spectra of the interferograms Figs. 3(a)

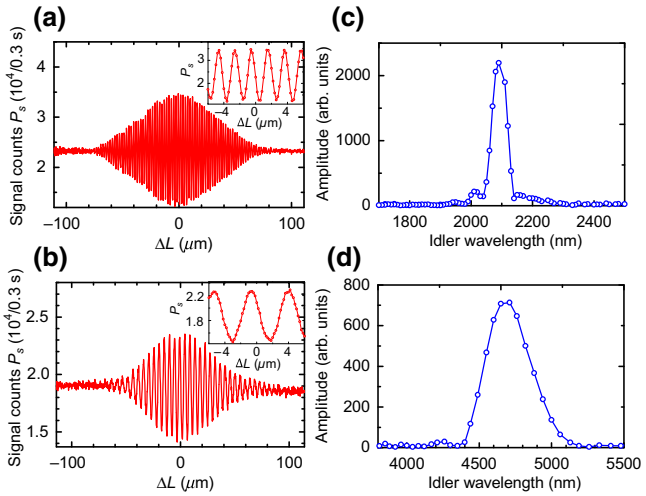

FIG. 3. Quantum interferograms of the detected signal counts P_s while scanning the optical path length difference ΔL by moving the idler mirror M_i, with signal and idler photon wavelengths of (a) 712 and 2104 nm and (b) 600 and 4694 nm. Fourier spectra (c),(d) of the quantum interferograms (a),(b), respectively.

and 3(b), respectively. The FWHM of the Fourier spectra in Fig. 3(d) is 344 nm while that in Fig. 3(c) is 51 nm. Figure 4 shows the idler central wavelength for each observed Fourier amplitude spectrum as a function of the internal angle θ' between the propagation direction of the pump beam and the optic axis in the crystal, determined from the rotation angle θ and the refractive index of the LN crystal at the pump wavelength [19]. Here, the idler central wavelengths are weighted by each Fourier spectral amplitude, and the theoretical curve is calculated from the relation between the wavelength of the pump, signal, and idler photons for the type-I collinear phase-matching condition and the Sellmeier dispersion equation for the

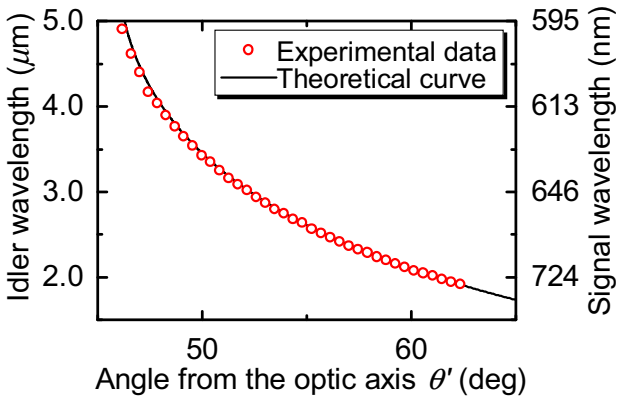

FIG. 4. Dependence of the idler central wavelength on the internal angle θ' between the propagation direction of the pump beam and the optic axis in the crystal. The right axis shows the corresponding wavelength of the signal photons.

LN crystal [21]. They are in good agreement in the wavelength range of 2–5 μm. These results show that with this IRQAS system, quantum interference can be continuously observed over the broad MIR region 2–5 μm by tuning the SPDC wavelengths by crystal rotation.

Next, we investigate the visibility of the quantum interference with the wavelength-tunable IRQAS system in the wavelength region of 2–5 μm. In the transmission spectrum of a sample, the visibility is directly connected to the SNR, which is a useful characteristic of an IRQAS system [16]. Figure 5 shows the wavelength dependence of the visibility of the quantum interferograms with crystal rotation in the wavelength range of 2–5 μm. The gray squares show the maximum visibility in the case where the alignment is adjusted for each idler wavelength with crystal rotation. We can see a decrease in the visibility around a wavelength of 3 μm and in the wavelength region longer than 4 μm. This is caused by absorption by the LN crystal [22]. Next, we align the system to maximize the visibility at an idler wavelength of 3.6 μm and investigate how the visibility changes as the SPDC wavelength is scanned over the operable MIR range without any realignment (circles). It can be seen that the visibility for the fixed alignment decreases as the rotation angle is changed from a fixed wavelength of 3.6 μm, and is lower than the visibility for realignment at each idler wavelength. This is due to the displacement of the optical paths of the pump, signal, and idler photons due to crystal rotation. However, even without realignment of the system, the visibility remains relatively high above 25% for an idler wavelength of less than 4 μm, and we can also clearly see quantum interference even around 5 μm. These results indicate that we can

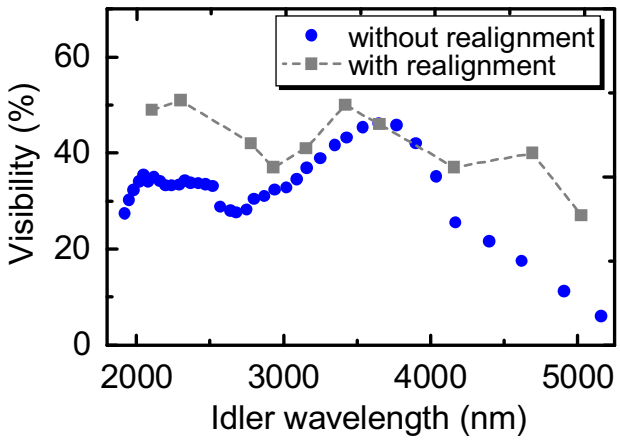

FIG. 5. Wavelength dependence of the visibility of the quantum interferograms. The circles show the visibility in the case where the alignment of the collimation lens L2 in the idler path is adjusted and then fixed at an idler wavelength of 3.6 μm. The squares are the visibility when the alignment is adjusted for each idler wavelength.

perform alignment-free IRQAS measurements over a wide MIR region 2–5 μm.

B. Rapid transmission spectrum measurement of the fused silica sample with the coarse-scan method

Next, for the transmittance measurement of a sample, we insert a UVFS sample into the interferometer arm for idler photons and observe the change in the quantum interferograms. As described in the previous section, with the coarse-scan method, it is possible to obtain the transmittance for a sample from the ratio of the visibilities with and without a sample. Because the visibility is affected by the dispersion in the sample, we first investigate the effect of dispersion in the UVFS sample on the visibility of the quantum interferogram. We assume that the spectral profile for the biphotons $F(\omega_i)$ is a Gaussian function $(\tau/2\sqrt{\pi})e^{-\tau^2(\omega_i-\omega_{i0})^2/4}$, where τ is the coherence time for the SPDC estimated from the central frequency and the FWHM, and the quantum interferogram in the time domain without a sample is a transform-limited Gaussian pulse. We consider the effect only due to the group-velocity dispersion β'' for the sample as a dispersion medium. The GVD of the UVFS is calculated from the Sellmeier dispersion equation, which is valid for wavelengths from 0.21 to 3.71 μm. When the idler wavelength is 3652 nm and the FWHM is 54 nm, the group-delay dispersion (GDD) for the sample is -2570 fs^2. Using this value and Eqs. (2) and (3), we calculate the visibility of the quantum interferogram P_s for a sample transmittance of $T = 1$, and then obtained a value of approximately 1 (0.9997). This result shows that the quantum interferogram is almost unaffected by the GVD of the UVFS sample in this wavelength region. Therefore, in the following, the transmittance of the sample is simply measured from the ratio of the visibilities with and without the sample using the coarse-scan method.

Next, we perform a high-speed transmission spectrum measurement from the ratio of the visibility of quantum interferograms with and without a sample while tuning the SPDC wavelengths by crystal rotation. We follow the coarse-scan approach detailed in Sec. II. Figure 6 shows the transmittance spectra of the UVFS sample measured by conventional FTIR spectroscopy (solid line) with a resolution of 4 cm^{-1}, where the large and small dips around the wavelengths of 2.7 μm and 4.3 μm are caused by absorption due to OH stretching of impurities in the sample [23], and the wavelength-tunable IRQAS system (circles). Note that to extract the interference visibility, the data for two periods of the interference around zero ΔL for each quantum interferogram are fitted using a sine function given by $y = y_0 + A\sin[\pi\,(x-b)/d]$, where the fitting parameters are an offset y_0, an amplitude A, a central position b, and an interference period of d. The error bars for the transmission spectrum data (circles) represent error propagation in the fitting process. In addition, the wavelengths for each data point (circles) are spectral centroids determined from each Fourier spectral amplitude without the sample. The results clearly show that the large dip in the transmission spectrum around a wavelength of 2.7 μm due to OH stretching could be measured with the IRQAS system. The discrepancy between the IRQAS and conventional FTIR spectroscopy measurement results around the wavelength of 4.5 μm is due to the difference in the spectral resolutions of each system; for the coarse-scan method (as discussed in the previous section), the spectral resolution is limited by the finite bandwidth of the SPDC photon pairs. For a fair comparison, the transmission spectrum measured by conventional FTIR spectroscopy is averaged with each Fourier amplitude spectra of quantum interferograms with each tuning angle (squares). The transmission spectrum measured by the IRQAS system is in good agreement with the weighted average transmission spectrum measured by conventional FTIR spectroscopy in the broad MIR region 1.9–5.2 μm. These results clearly show that this IRQAS system can perform wavelength-tunable transmission spectrum measurements in the wavelength region 2–5 μm. In this experiment, the integration time is 50 ms and the step size for the idler mirror is 100 nm. The visibility could be obtained from the data around zero delay in two periods of the quantum interference corresponding to idler wavelengths of 2–5 μm. In this case, the step number is 20–50, so the acquisition time is 1.0–2.5 s. Therefore, the total measurement time for the data in Fig. 6 is about 240 s. To further improve the acquisition speed, it is possible to increase the scanning step size to obtain the visibility.

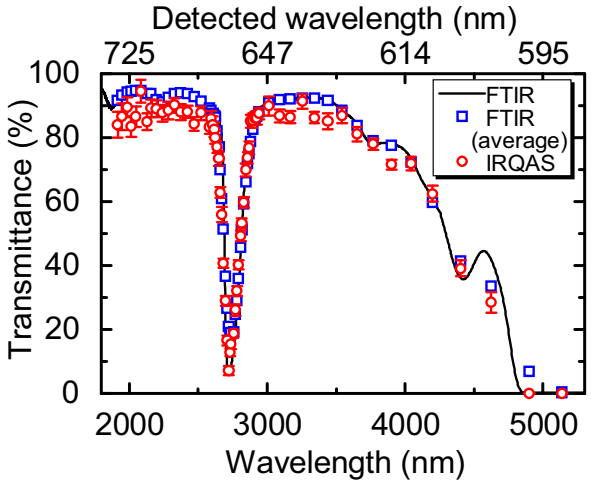

FIG. 6. Transmission spectrum of a UVFS sample measured by conventional FTIR spectroscopy (solid line) and the wavelength-tunable IRQAS system in this work (circles). The squares show the weighted average value of the transmission spectrum with the intensity of the SPDC spectrum obtained from a Fourier analysis of the quantum interferograms. The error bars show the standard errors for the average values.

In addition, by improving the photon-pair generation rate using a quasi-phase-matching device [24], the integration time can be reduced while the SNR is maintained.

C. High-resolution QFTIR with the fine-scan method

As shown in the previous section and the experimental demonstration, in the coarse-scan method, the resolution of the measurement is limited by the finite bandwidth of each SPDC spectrum. Thus, we next perform a transmittance measurement with a higher resolution within the SPDC spectrum with wavelength-tunable QFTIR (fine scan). We focus on wavelengths of 2.7 and 4.3 μm around the OH-stretching absorption band for the UVFS sample. To improve the resolution, we change M_i in steps of 100 nm (corresponding to a change in ΔL of 200 nm) up to a total scanning length W of 1200 μm. The integration time is 50 ms for each step. We obtain the Fourier amplitude spectra from a Fourier analysis of the quantum interferograms. Figures 7(a) and 7(b) show the Fourier amplitude spectra without the sample for various crystal rotation angles in the wavelength regions around 2.7 and 4.3 μm, respectively. With QFTIR, the transmittance of a sample can be evaluated from the ratio of the Fourier amplitude without and with a sample at each wavelength.

We measure the transmittance of the UVFS sample with the fine-scan method while continuously tuning the SPDC wavelength by crystal rotation around the wavelengths of 2.7 and 4.3 μm, corresponding to wavelengths of the OH-stretching absorption for the sample. Figures 7(c) and 7(d) show the transmission spectra of the sample around these wavelengths. The solid line shows the transmission spectrum measured by conventional FTIR, indicating good agreement in the wavelength regions 2.7–2.9 and 3.9–4.8 μm. The resolution of these measurements Δk is 8.33 cm^{-1} ($\Delta k = 1/W$). These results show that high-resolution transmittance measurements can be performed in an arbitrary wavelength region with wavelength-tunable QFTIR.

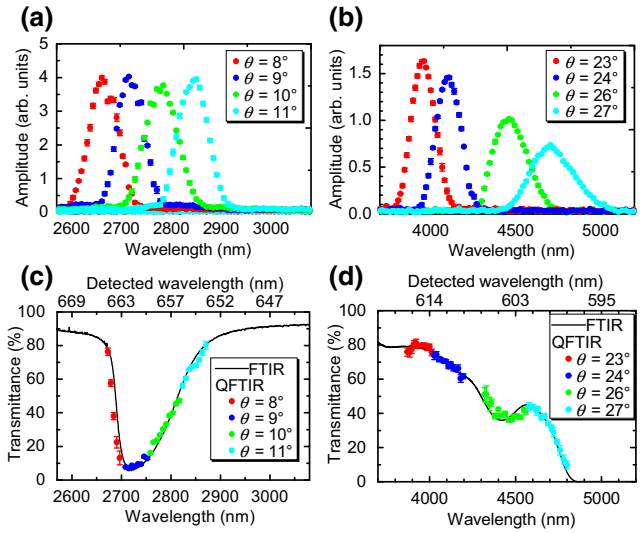

FIG. 7. Fourier spectra of quantum interferograms without a UVFS sample with rotation angles (a) from $\theta = 8^\circ$ to 11° and (b) from $\theta = 23^\circ$ to 27°. Transmission spectrum of a UVFS sample by QFTIR (red, dark blue, green, and light blue) and conventional FTIR spectroscopy (black line) (c),(d) evaluated from Figs. 7(a) and 7(b), respectively. The error bars show standard errors estimated from five measurements.

V. CONCLUSION

We experimentally demonstrate a wavelength-tunable IRQAS system covering the whole MIR region 1.9–5.2 μm. The SPDC wavelengths can be tuned over a wide spectral region by changing the angle of a nonlinear crystal. The wavelengths of midinfrared photons estimated from the Fourier spectra of the quantum interferograms agreed well with the theoretical predictions for the given angles of the nonlinear crystal. First, we investigate the crystal rotation dependence of the visibility of the quantum interference. The results show that the visibility is sufficiently high in the wavelength region 2–5 μm even without fine realignment. Next, we demonstrate a method for high-speed transmission spectrum measurement of a UVFS sample from the ratio of the visibilities of two periods of quantum interference with and without the sample. The results agreed well with the spectrum measured by conventional FTIR spectroscopy over the whole MIR region 1.9–5.2 μm. We demonstrate a short total measurement time of 240 s for the whole transmission spectrum. Furthermore, to improve the resolution of the measurement, we perform a transmittance measurement based on QFTIR with a high resolution of 8.33 cm^{-1} in the wavelength region of 2.7–2.9 and 3.9–4.8 μm. The measured transmittance is in good agreement with that measured by conventional FTIR spectroscopy. These results show that high-resolution transmittance measurements can also be performed for arbitrary wavelength regions with QFTIR.

We believe that the experimental realization of the ultrabroadband tunable IRQAS system reported here is a milestone for the use of the IRQAS system in real-world applications since the reported principle can also be adaptable for different wavelength regions from visible to farinfrared using different types of nonlinear crystals and even with quasi-phase-matching devices for higher SPDC efficiencies. Although the improvement in the efficiency of the entangled photon sources will make the SNR of the IRQAS system comparable to or even overcome that of the traditional infrared spectrometers, SNR of the IRQAS system reported in this paper outperforms a conventional spectrometer when the irradiated light power to the sample is taken into account (assuming Poisson statistics of the probe light as the main noise source). In this sense, the current system with just less than pW

level probe light intensity, is already useful for applications, which requires invasive measurements. This IRQAS system thus will have future potential applications in a variety of fields ranging from condensed-matter physics to biomedical sciences.

ACKNOWLEDGMENTS

This work is supported by MEXT Quantum Leap Flagship Program (MEXT Q-LEAP) Grant No. JPMXS011806 7634, Cabinet Office, Government of Japan, Public/Private R&D Investment Strategic Expansion Program (PRISM), JST-CREST Grant No. JPMJCR1674, JST-PRESTO Grant No. JPMJPR15P4, JSPS KAKENHI Grant No. 21H04444, and Grant-in-Aid for JSPS Fellows Grant No. 20J23408, and WISE Program, MEXT.

[1] B. Stuart, *Infrared Spectroscopy: Fundamentals and Applications* (Wiley, Chichester, UK, 2004).
[2] B. C. Smith, *Fundamentals of Fourier Transform Infrared Spectroscopy* (CRC Press, Boca Raton, FL, 2011), 2nd ed.
[3] D. A. Kalashnikov, A. V. Paterova, S. P. Kulik, and L. A. Krivitsky, Infrared spectroscopy with visible light, Nat. Photonics **10**, 98 (2016).
[4] T. Nagata, R. Okamoto, J. L. O'Brien, K. Sasaki, and S. Takeuchi, Beating the standard quantum limit with four-entangled photons, Science **316**, 726 (2007).
[5] V. Giovannetti, S. Lloyd, and L. Maccone, Advances in quantum metrology, Nat. Photonics **5**, 222 (2011).
[6] T. Ono, R. Okamoto, and S. Takeuchi, An entanglement-enhanced microscope, Nat. Commun. **4**, 2426 (2013).
[7] R. Z. Vered, Y. Shaked, Y. Ben-Or, M. Rosenbluh, and A. Pe'er, Classical-to-Quantum Transition with Broadband Four-Wave Mixing, Phys. Rev. Lett. **114**, 063902 (2015).
[8] Z. Y. Ou and X. Li, Quantum SU(1, 1) interferometers: Basic principles and applications, APL Photonics **5**, 080902 (2020).
[9] Y. Mukai, M. Arahata, T. Tashima, R. Okamoto, and S. Takeuchi, Quantum Fourier-Transform Infrared Spectroscopy for Complex Transmittance Measurements, Phys. Rev. Appl. **15**, 034019 (2021).
[10] B. Yurke, S. L. McCall, and J. R. Klauder, SU(2) and SU(1, 1) interferometers, Phys. Rev. A **33**, 4033 (1986).
[11] M. V. Chekhova and Z. Y. Ou, Nonlinear interferometers in quantum optics, Adv. Opt. Photonics **8**, 104 (2016).
[12] A. V. Paterova, S. M. Maniam, H. Yang, G. Grenci, and L. A. Krivitsky, Hyperspectral infrared microscopy with visible light, Sci. Adv. **6**, eabd0460 (2020).
[13] I. Kviatkovsky, H. M. Chrzanowski, E. G. Avery, H. Bartolomaeus, and S. Ramelow, Microscopy with undetected photons in the mid-infrared, Sci. Adv. **6**, eabd0264 (2020).
[14] A. Vanselow, P. Kaufmann, I. Zorin, B. Heise, H. M. Chrzanowski, and S. Ramelow, Frequency-domain optical coherence tomography with undetected mid-infrared photons, Optica **7**, 1729 (2020).
[15] C. Lindner, S. Wolf, J. Kiessling, and F. Kühnemann, Fourier transform infrared spectroscopy with visible light, Opt. Express **28**, 4426 (2020).
[16] C. Lindner, J. Kunz, S. J. Herr, S. Wolf, J. Kiessling, and F. Kühnemann, Nonlinear interferometer for Fourier-transform mid-infrared gas spectroscopy using near-infrared detection, Opt. Express **29**, 4035 (2021).
[17] A. Vanselow, P. Kaufmann, H. M. Chrzanowski, and S. Ramelow, Ultra-broadband SPDC for spectrally far separated photon pairs, Opt. Lett. **44**, 4638 (2019).
[18] P. Kaufmann, H. M. Chrzanowski, A. Vanselow, and S. Ramelow, Mid-IR spectroscopy with NIR grating spectrometers, Opt. Express **30**, 5926 (2022).
[19] M. Arahata, Y. Mukai, B. Cao, T. Tashima, R. Okamoto, and S. Takeuchi, Wavelength variable generation and detection of photon pairs in visible and mid-infrared regions via spontaneous parametric downconversion, J. Opt. Soc. Am. B **38**, 6 (2021).
[20] A. Paterova, H. Yang, C. An, D. Kalashnikov, and L. Krivitsky, Measurement of infrared optical constants with visible photons, New J. Phys. **20**, 043015 (2018).
[21] D. E. Zelmon, D. L. Small, and D. Jundt, Infrared corrected sellmeier coefficients for congruently grown lithium niobate and 5 mol.% magnesium oxide-doped lithium niobate, J. Opt. Soc. Am. B **14**, 3319 (1997).
[22] M. Leidinger, S. Fieberg, N. Waasem, F. Kuhnemann, K. Buse, and I. Breunig, Comparative study on three highly sensitive absorption measurement techniques characterizing lithium niobate over its entire transparent spectral range, Opt. Express **23**, 21690 (2015).
[23] G. E. Walrafen and S. R. Samanta, Infrared absorbance spectra and interactions involving OH groups in fused silica, J. Chem. Phys. **69**, 493 (1978).
[24] B. Cao, M. Hisamitsu, K. Tokuda, S. Kurimura, R. Okamoto, and S. Takeuchi, Efficient generation of ultra-broadband parametric fluorescence using chirped quasi-phase-matched waveguide devices, Opt. Express **29**, 21615 (2021).